1.3-GHz Superconducting Radio Frequency Cavity Stress and Buckling Analysis

1. Cryomodule Assembly

The International Linear Collider (ILC) is an electron-positron collider accelerator, that requires approximately 7800 1.3 GHz Niobium 9-cell cavities to attain 250 GeV centre-of-mass energy and is extendable up to 1 TeV [1, 2]. The ILC will be a 31 km long linear collider whose major sub-system will include photocathode DC gun, polarized positron source, electron and positron damping rings, beam transport from damping rings to the main linacs, two 11 km main linacs utilizing 1.3 GHz 9-Cell superconducting radio frequency cavities (SRF) operating at an average gradient of 31.5 MV/m, two beam delivery systems each 2.2 km long and cryogenic plants to cool down the cryomodules. The 7800 cavities will be housed in approximately 850 cryomodules, which are roughly 12.65 m long [2].

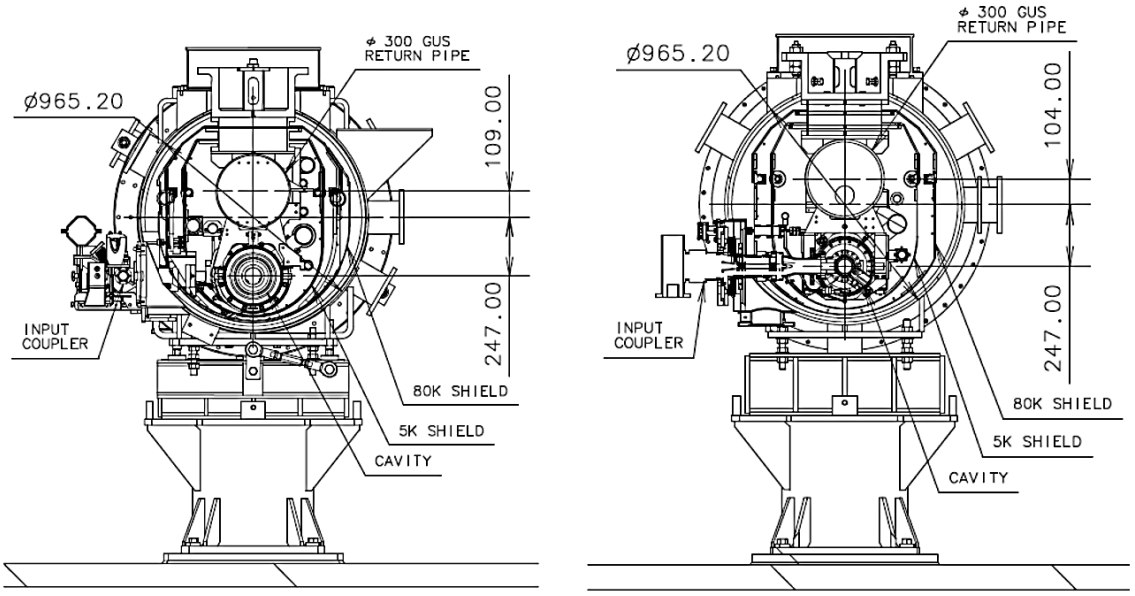

(a) Module-C for FNAL cavity (b) Module-A for KEK cavity

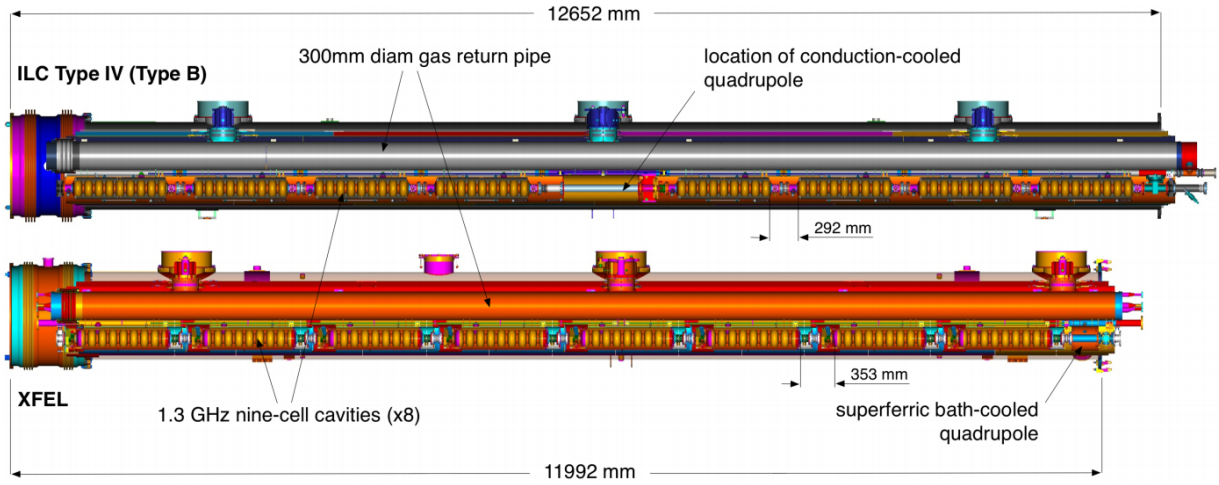

Fig. 1 Example of cryomodule cross-section for FNAL and KEK (Top) [3]; Different types of cryomodules, ILC and Eu-XFEL design [2] (below)

There are two types of cryomodules for ILC: a Type A module with nine 1.3 GHz nine-cell cavities and Type B with eight nine-cell cavities and one superconducting quadrupole package located at the centre of the module, an example of a cryomodule is shown in Fig. 1 (below). The cryomodule consists of cavity packages, input couplers, the gas return pipe (GRP), magnetic shields, two sets of thermal shields, cooling pipes and the vacuum vessel. The cooling pipes includes the 2 K two-phase superfluid helium pipeline, 2 K gas helium return line (Φ 300 mm), 5 K shield line and 80 K or 40 K shield line. The cold mass at 2 K is enclosed with two thermal shields at 5 K and 40 K which are cooled with LHe (liquid helium) [2]. A cross-sectional view of cryomodule is shown in Fig. 1a.

2. Pressure Vessel Compliance for Cryomodules

The cryomodule has components that can be considered as pressure vessels and needs to be cleared by high-pressure gas safety authorities for operation. Most of the components like the 2 K GHe return line, 2 K two-phase line, 5 K thermal shield line and 80 K thermal shield line are stainless steel (SUS316L) pipes which doesn't create any issues with clearing high pressure safety regulations. However, the SRF cavities are constructed of Niobium and encased in a Ti helium jacket, which is filled with superfluid helium (another phase of liquid helium) at 2.0 K for its operational conditions, hence the assembly is considered as a pressure vessel [3]. The materials such as Niobium, Titanium and NbTi alloys are not approved for pressure vessel design due to the lack of code data in high pressure codes, for room temperature and cryogenic temperatures (at 4.21 K or below). Hence, to operate the SRF cavity assembly it is necessary to show certain level of safety which is greater than or at least equal to acceptable standards to the high-pressure gas safety authorities for the cavity operation.

2.1.1. 1.3 GHz SRF Cavity Assembly

There are currently two types of 1.3 GHz SRF cavity design in operation: Tesla and Tesla-like cavities. The difference between the shapes of the cavity is minuscule but the design of the Titanium Jacket, end group and Tuner varies in many facilities. The current Tuner and Ti Jacket design proposed for ILC's SRF cavities is shown in the Fig. 2 (below) and its cut section view in Fig. 2 (top).

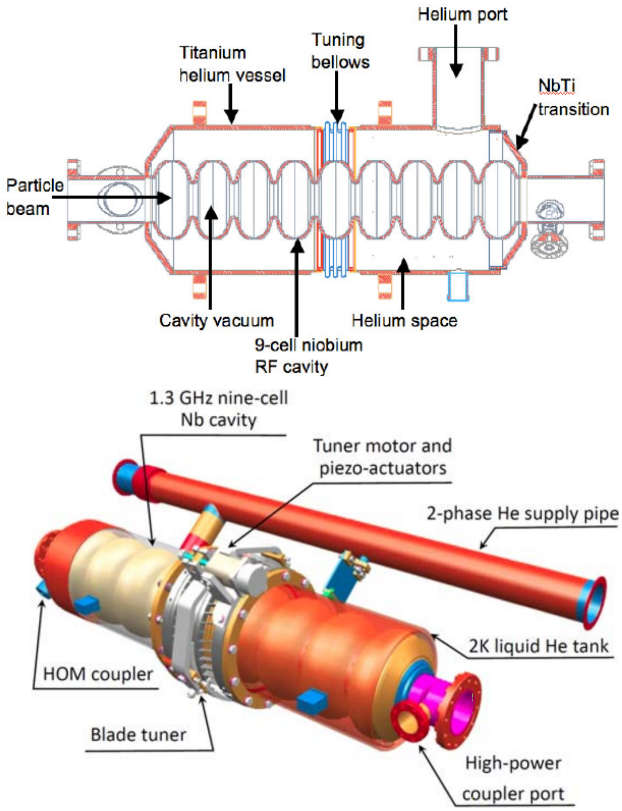

Fig. 2 Illustration of a 1.3 GHz Nb SRF cavity assembly (top) [3]; 1.3 GHz SRF cavity assembly for ILC (below) [2]

The largest accelerator operating the Tesla cavities is the European Free Electron Laser (EU-XFEL). It is a 2.1 km superconducting Linac to accelerate electron to 17 GeV by using

808 1.3 GHz 9-Cell SRF cavities [4]. Design of the Eu-XFEL's 1.3 GHz Tesla cavity assembly is shown in the Fig. 3.

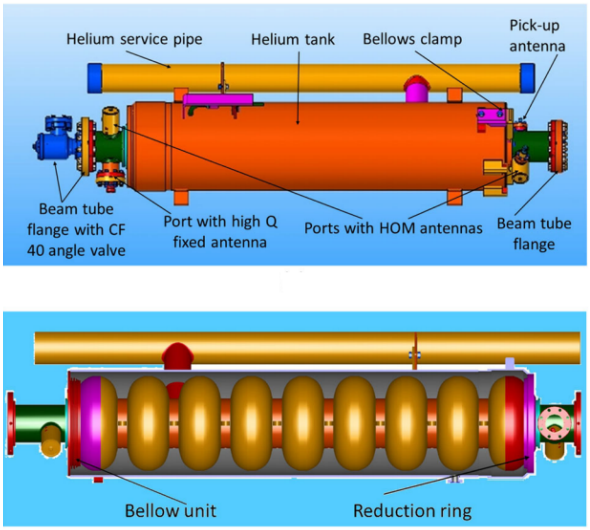

Fig. 3 Tesla cavity assemble at Eu-XFEL DESY (top) and its cut view (below) [4]

3. Structural Analysis

3.1. Structural Analysis using FEA [5]

The FEA is a powerful computational technique for approximate solutions to a variety of "real-world" problems. It relies on decomposition of domain (solid, liquid or gas) into a finite number of sub-domains for which systematic approximate solution is constructed by applying the variational or weighted residual methods. FEA reduces the problem into finite number of unknowns by dividing the domain into elements and by expressing the unknown field variable in terms of the assumed approximating functions within each element. These functions are also called interpolating functions are defined in terms of the values of the field variables at specific points, referred as nodes which are located along the element boundaries and connects the adjacent elements. The ability to discretize the irregular domains with finite elements makes the method a valuable and practical analysis tool for the solution of boundary, initial, and eigenvalue problems in various engineering disciplines [5]. The FEA method requires following steps.

- Discretization of the domain into finite number of sub-domains.
- Selection of interpolating functions.
- Development of the elemental matrix of the sub-domain.
- Assembly of the element matrices for each subdomain to obtain global matrix for the entire domain.
- Imposition of boundary conditions.
- Solution of equations.
- Additional data-analysis if necessary.

In matrix notation, the global system of equations can be cast into:

$$Ku = F, \qquad (3-1)$$

Where K is the system stiffness matrix, u is the vector of unknowns, and F is the force vector. Depending on the nature of problem, K maybe be dependent on u and F maybe time dependent, i.e., F = F(t) [5].

3.1.1. Nodes

A node specifies the coordinate location in space where degrees of freedom and actions of the physical problem exist. The nodal unknowns in the matrix system of equations represents on or more of the primary field variables. Nodal variables assigned to an element are called degrees of freedom (DOF) of the element. The common nodes provide the continuity for the nodal variables. DOF of a node is dictated by the physical nature of a problem and the element type [5].

3.1.2. Elements

The geometry can be discretized considering the complexity of shape and the physical nature of the problem. There are various methods of

discretization methodologies like line element for 1D problems, area elements like triangular, rectangular and quadrilaterals for 2D problems and tetrahedrals, prisms and hexahedrals for volume elements. The elements are identified by element numbers and is defined by a specific sequence of global node numbers, as shown in Fig. 4 [5].

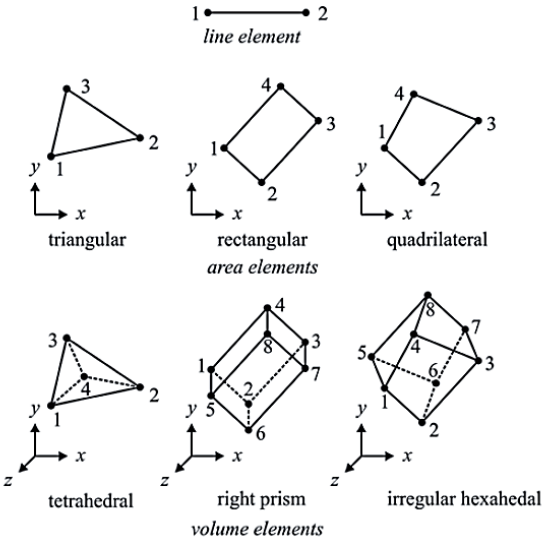

Fig. 4 line, area and volume elements with node numbers at element level [5]

3.2. Direct Approach for FEA

3.2.1. Linear Spring System

It is suitable for simpler problems but is fundamental step of a typical finite element analysis. In this approach a linear spring system is considered in 1-D domain [5]. As shown in Fig. 5, a linear spring with stiffness k has two nodes and each nodes is subjected to axial loads of f_1 and f_2 resulting in displacement of u_1 and u_2 in their defined positive direction.

Due to the defined nodal forces the resulting displacement is,

$$\mathrm{u} = u_1 - u_2, \qquad (3-2)$$

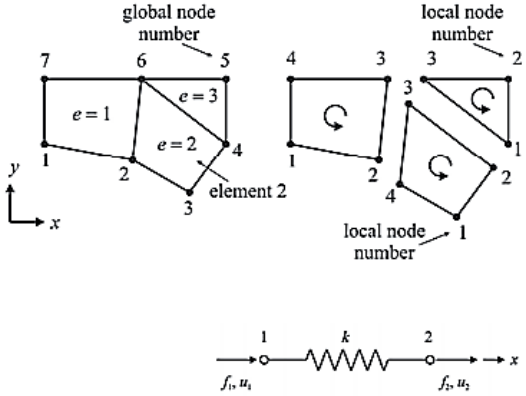

Fig. 5 Discretization of a domain: element and node (Top); free-body diagram of a linear spring element (bottom) [5]

This is related to force acting on the spring

$$f_1 = \mathrm{ku} = \mathrm{k}(u_1 - u_2), \qquad (3-3)$$

The equilibrium of forces requires that

$$f_2 = -f_1, \qquad (3-4)$$

Which yields

$$f_2 = \mathrm{k}(u_2 - u_1), \qquad (3-5)$$

Combining equation 3-3 and 3-5 and rewriting the equations in matrix form, we get

$$\begin{bmatrix} k & -k \\ -k & k \end{bmatrix} \begin{Bmatrix} u_1 \\ u_2 \end{Bmatrix} = \begin{Bmatrix} f_1 \\ f_2 \end{Bmatrix} \text{ or } k^{(e)} u^{(e)} = f^{(e)}. \qquad (3-6)$$

Here, $u^{(e)}$ is the vector of nodal unknowns representing displacement, $k^{(e)}$ is the element (stiffness) matrix and $f^{(e)}$ is the element (force) vector. The stiffness matrix can be represented in its indicial form as $k_{ij}^{(e)}$,

$$k^{(e)} \sim k_{ij}^{(e)}. \qquad (3-7)$$

where i and j are the row and the column numbers. The coefficients, $k_{ij}^{(e)}$, may be interpreted as the force required at node i to produce unit displacement in node j while all the other nodes are fixed [5].

3.2.2. Assembly of the Global System of Equations

To model an engineering problem with finite elements requires the assembly of element characteristic (stiffness) matrices and element right-hand-side vectors, leading the global system of equations, as equation 3-1 [5].

$$\mathrm{Ku} = \mathrm{F}, \qquad (3-8)$$

The global system matrix, K, can be obtained from the "expanded" element coefficient matrices, $k^{(e)}$, by summation in the form

$$\mathrm{K} = \sum_{e=1}^{E} k^{(e)}, \qquad (3-9)$$

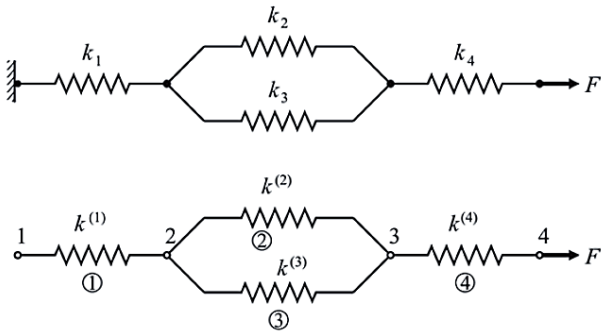

Fig. 6 System of linear springs (top) and corresponding FEA (below) [5]

The parameter E denotes the number of elements and the expanded element characteristic matrices are the same size as the global system matrix but have the rows and columns of zeros corresponding to the nodes not associated with element (e). Similarly, the global right hand side vector, F, can be obtained from the expanded element coefficient vectors, $f^{(e)}$, by summation in the form given below, and the size of the global right-hand-side vector is also dictated by the highest number among the global node numbers [5].

$$\mathrm{F} = \sum_{e=1}^{E} f^{(e)}, \qquad (3-10)$$

The global system matrix and the global right-hand-side vector are constructed by considering the systems of linear springs shown in Fig. 6. For an element equations for a spring is given by equation 3-6 and rewritten as [5]

$$\begin{bmatrix} k_{11}^{(e)} & k_{12}^{(e)} \\ k_{21}^{(e)} & k_{22}^{(e)} \end{bmatrix} \begin{Bmatrix} u_1^{(e)} \\ u_2^{(e)} \end{Bmatrix} = \begin{Bmatrix} f_1^{(e)} \\ f_2^{(e)} \end{Bmatrix}. \qquad (3-11)$$

In which $k_{11}^{(e)} = k_{22}^{(e)} = k^{(e)}$ and $k_{21}^{(e)} = k_{12}^{(e)} = -k^{(e)}$. The subscripts corresponds to Node 1 and 2. In accordance with equation 3-8 and 3-9 the global system matrix is (4×4) and is shown below [5]

$$\mathrm{K} = \begin{bmatrix} k_{11}^{(1)} & k_{12}^{(1)} & 0 & 0 \\ k_{21}^{(e)} & \begin{pmatrix} k_{22}^{(1)} + k_{11}^{(2)} \\ +k_{11}^{(3)} \end{pmatrix} & \left(k_{12}^{(2)} + k_{12}^{(3)}\right) & 0 \\ 0 & \left(k_{21}^{(2)} + k_{21}^{(3)}\right) & \begin{pmatrix} k_{22}^{(2)} + k_{22}^{(3)} \\ +k_{11}^{(4)} \end{pmatrix} & k_{12}^{(e)} \\ 0 & 0 & k_{21}^{(e)} & k_{22}^{(4)} \end{bmatrix}, \qquad (3-12)$$

And the global right-hand-side vector is (4×1) and the contribution of each element is summed as

$$\mathrm{K} = \begin{bmatrix} f_1 \\ f_2 \\ f_3 \\ f_4 \end{bmatrix} = \begin{bmatrix} f_1^{(1)} \\ f_2^{(1)} + f_1^{(2)} + f_1^{(3)} \\ f_2^{(2)} + f_2^{(3)} + f_1^{(4)} \\ f_2^{(4)} \end{bmatrix}. \qquad (3-13)$$

And the vector of unknowns, u, becomes

$$\mathrm{u} = \begin{bmatrix} u_1 \\ u_2 \\ u_3 \\ u_4 \end{bmatrix} = \begin{bmatrix} u_1^{(1)} \\ u_2^{(1)} = u_1^{(2)} = u_1^{(3)} \\ u_2^{(2)} = u_2^{(3)} = u_1^{(4)} \\ u_2^{(4)} \end{bmatrix}. \qquad (3-14)$$

For the specific values $k_{11}^{(e)} = k_{22}^{(e)} = k^{(e)}$ and $k_{21}^{(e)} = k_{12}^{(e)} = -k^{(e)}$, the global system matrix becomes

$$\mathrm{K} = k^{(e)} \begin{bmatrix} 1 & -1 & 0 & 0 \\ -1 & 3 & -2 & 0 \\ 0 & -2 & 3 & -1 \\ 0 & 0 & -1 & 1 \end{bmatrix}. \qquad (3-15)$$

The eigenvalues are $\lambda_1 = 0, \lambda_2 = 2, \lambda_3 = 3 - \sqrt{5}, \text{and } \lambda_3 = 3 - \sqrt{5}$. The corresponding eigenvectors are

$$\mathrm{u}^{(1)} = \begin{bmatrix} 1 \\ 1 \\ 1 \\ 1 \end{bmatrix}, \mathrm{u}^{(2)} = \begin{bmatrix} 1 \\ -1 \\ -1 \\ 1 \end{bmatrix},$$
$$\mathrm{u}^{(3)} = \begin{bmatrix} 1 \\ 2-\sqrt{5} \\ -2+\sqrt{5} \\ 1 \end{bmatrix}, \mathrm{u}^{(4)} = \begin{bmatrix} 1 \\ 2+\sqrt{5} \\ -2-\sqrt{5} \\ 1 \end{bmatrix}. \qquad (3-16)$$

Each of the eigenvectors represents a possible solution mode and their contribution is illustrated in Fig. 7.

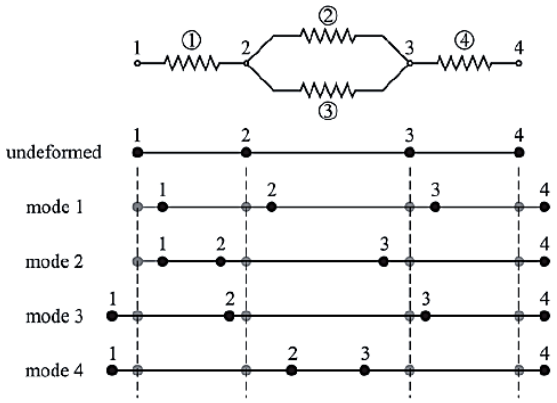

Fig. 7 possible solution modes for the system of linear springs [5]

In order to have unique solution, the global system matrix is rendered non-singular by eliminating the zero eigenvalue. This is achieved by introducing boundary condition to suppress the translational mode of the solution corresponding to the zero eigenvalue [5].

If a boundary condition is imposed like $u_1 = 0$, the nodal force f_1 still remains an unknown and other nodal displacements are unknowns, and the corresponding nodal forces have values of $f_1 = 0,\ f_2 = f_3 = 0,$ and $f_4 = F$. Then the global system of equations are written as

$$k^{(e)} \begin{bmatrix} 1 & -1 & 0 & 0 \\ -1 & 3 & -2 & 0 \\ 0 & -2 & 3 & -1 \\ 0 & 0 & -1 & 1 \end{bmatrix} \begin{bmatrix} 0 \\ u_2 \\ u_3 \\ u_4 \end{bmatrix} = \begin{bmatrix} f_1 \\ 0 \\ 0 \\ F \end{bmatrix}, \qquad (3-17)$$

Leading to following solutions

$$-k^{(e)} u_2 = f_1, \qquad (3-18)$$

And

$$u_2 = \frac{F}{k^{(e)}}, u_3 = \frac{3}{2}\frac{F}{k^{(e)}}, u_4 = \frac{5}{2}\frac{F}{k^{(e)}}. \qquad (3-19)$$

And the unknown nodal force f_1 is determined as $f_1 = -F$. The physically acceptable solution mode is shown in Fig. 8 below.

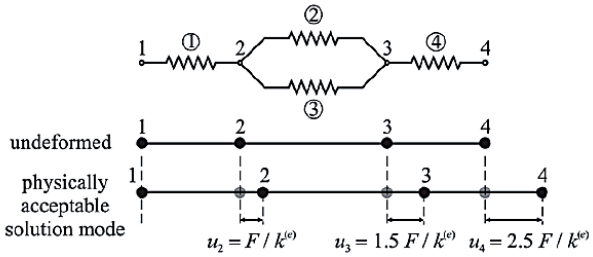

Fig. 8 Physically acceptable solution mode for the system of linear springs [5]

3.3. FEA with ANSYS® Simulation Software

In this section, we will investigate the theory behind the structure analysis conducted using ANSYS® Mechanical APDL. This section is basically an outline of the theory behind structural analysis without material and geometric nonlinearities. It was referenced from ANSYS® Mechanical APDL theory reference [6].

In this analysis, the applied load and the boundary conditions doesn't change with time. However, material and geometrical non-

linearities can be modeled, such as material plasticity, creeping phenomenon etc. In terms of SRF cavity, we would like to know the stress at which the cavity structure will permanently change (stress intensity > 0.2% yield strength), rendering its structure permanently deformed.

3.3.1. Stress-strain Relationship in ANSYS®

The stress and strain for linear materials are related through the following equation and the stress vectors are shown in Fig. 9 [6]:

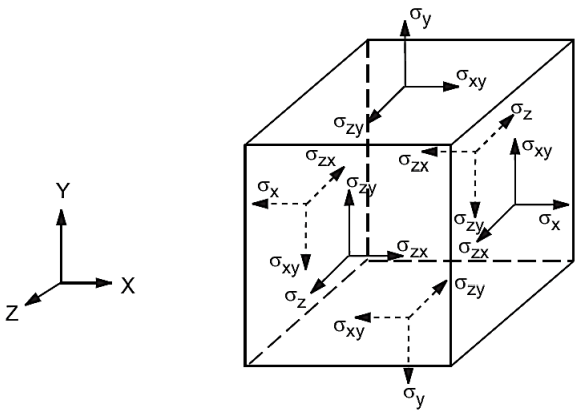

Fig. 9 Stress vector definition [6]

$$\{\sigma\} = D\{\varepsilon^{el}\}, \qquad (3-20)$$

where:

$\{\sigma\}$ = Stress vector = $[\sigma_x\ \sigma_y\ \sigma_z\ \sigma_{xy}\ \sigma_{yz}\ \sigma_{xz}]^T$

[D] = Elasticity or elastic stiffness matrix or stress-strain matrix.

$\{\varepsilon^{el}\} = \{\varepsilon\} - \{\varepsilon^{th}\}$ = elastic strain vector

$\{\varepsilon\}$ = total strain vector = $[\varepsilon_x\ \varepsilon_y\ \varepsilon_z\ \varepsilon_{xy}\ \varepsilon_{yz}\ \varepsilon_{xz}]^T$

$\{\varepsilon^{th}\}$ = thermal strain vector

The equation 3-20 can be inverted to:

$$\{\varepsilon\} = \{\varepsilon^{th}\} + [D]^{-1}\{\sigma\}, \qquad (3-21)$$

For the 3-D case, the thermal strain vector is:

$$\{\varepsilon^{th}\} = \Delta T[\alpha_x^{se}\ \alpha_y^{se}\ \alpha_z^{se}\ 0\ 0\ 0]^T, \qquad (3-22)$$

where:

α_x^{se} = Secant coefficient of thermal expansion in the x direction

$\Delta T = T - T_{ref}$

T = current temperature at the point in question

T_{ref} = reference strain free temperature

The flexibility or compliance matrix is:

$$[\mathrm{D}]^{-1} = \begin{bmatrix} \frac{1}{E_x} & \frac{-\nu_{xy}}{E_x} & \frac{-\nu_{xz}}{E_x} & 0 & 0 & 0 \\ \frac{-\nu_{yx}}{E_y} & \frac{1}{E_y} & \frac{-\nu_{yz}}{E_y} & 0 & 0 & 0 \\ \frac{-\nu_{zx}}{E_z} & \frac{-\nu_{zy}}{E_z} & \frac{1}{E_z} & 0 & 0 & 0 \\ 0 & 0 & 0 & \frac{1}{G_{xy}} & 0 & 0 \\ 0 & 0 & 0 & 0 & \frac{1}{G_{yz}} & 0 \\ 0 & 0 & 0 & 0 & 0 & \frac{1}{G_{xz}} \end{bmatrix}. \qquad (3-23)$$

Where the typical terms are:

E_x = Young's modulus in the x direction

ν_{xy} = major Poisson's ratio

ν_{yx} = minor Poisson's ratio

G_{xy} = Shear modulus in the xy plane

The $[\mathrm{D}]^{-1}$ matrix is considered to be symmetric, so that:

$$\frac{\nu_{yx}}{E_y} = \frac{\nu_{xy}}{E_x}. \qquad (3-24)$$

$$\frac{\nu_{zx}}{E_z} = \frac{\nu_{xz}}{E_x}. \qquad (3-25)$$

$$\frac{\nu_{zy}}{E_z} = \frac{\nu_{yz}}{E_y}. \qquad (3-26)$$

The $\nu_{xy}, \nu_{yz}, \nu_{xz}, \nu_{yx}, \nu_{zy}\ and\ \nu_{zx}$ are not independent quantities because of above three relations and therefore at least one quantity is required from either side of the equation for orthotropic materials. In ANSYS®, it is assumed that E_x is larger than E_y, ν_{xy} is larger than ν_{yx}. Hence, ν_{xy} is referred as

"major' Poisson's ratio and ν_{yx} as "minor" Poisson's ratio. For isotropic materials ($E_x = E_y = E_z \; and \; \nu_{xy} = \nu_{yz} = \nu_{xz}$), so it doesn't make any difference with the provided data [6].

3.4. Eigenvalue Buckling

3.4.1. Euler's Buckling Load

The criteria for failure for a structure until now has been considered as the stress generated in a body due to its own weight or the external load should not exceed the yield stress of its construction material. However, when a structure has a dimension disproportionally larger than the others like a long slender beam, it is susceptible to failure under compressive force. The compressive force can be the structure's own weight or some kind of external force. The sheer size difference will cause the lateral deflection to be larger than the axial displacement called as buckling failure. This kind of failure is quite sudden and should be avoided for structure's integrity [7].

3.4.2. Euler Buckling Load for a pinned-pinned column

An example of buckling load for a pinned-pinned slender column subjected to axial forces at the ends is shown in this section. To determine the expression for buckling load, it is assumed that the column has already buckled and seek to determine the value of compressive force 'F' necessary to hold it in equilibrium. It is accomplished by proceeding to determine the distribution of the column's deflection in terms of F. In Fig. 10, a free-body diagram by passing a plane through the column at an arbitrary position x [7].

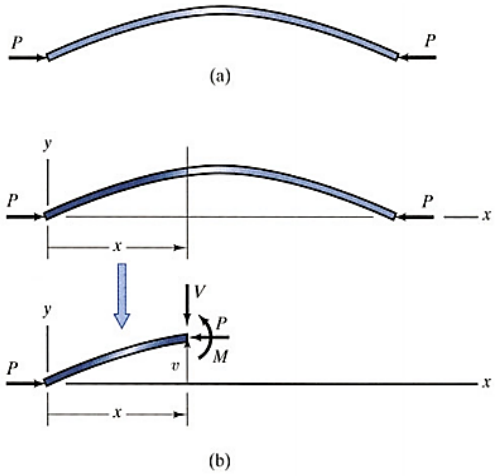

Fig. 10 Buckled column in equilibrium (a); determining bending moment as a function of x (b) [7]

The bending moment for the column is $M = -Fv$, where v the column's deflection at is x. Substituting this expression in a relationship between the beam's deflection and the bending moment $v'' = M/EI$ we get

$$v'' + \lambda^2 v = 0, \qquad (3-27)$$

Where

$$\lambda^2 = \frac{F}{EI}, \qquad (3-28)$$

Where EI is the flexural rigidity, E is the Young's modulus and I is the moment of inertia. The general solution of second order differential equation 3-27 is

$$v = B \sin \lambda x + C \cos x\,. \qquad (3-29)$$

Where B and C are constants. From the boundary condition that deflection is 0 at $x = 0, v|_{x=0} \; is \; 0,$ we get C = 0. The deflection is also 0 at $x = L$.

$$v|_{x=L} = 0, \qquad (3-30)$$

$$\text{B}\sin \lambda L = 0. \qquad (3-31)$$

If B = 0, then $v = 0$ which does satisfy equation 3-27 but we are seeking a buckled solution, hence if $B \neq 0$ then

$$\sin \lambda L = 0. \qquad (3-32)$$

The parameter λ depends on the compressive force F and equation 3-32 has infinite number of roots for λ. It is satisfied when

$$\lambda = \frac{n\pi}{L}. \qquad (3-33)$$

Where n is any integer.

Substituting equation 3-33 into 3-28 and 3-29, we obtain axial load as in equation 3-34 and deflection as in equation 3-35, with various modes of deflections shown in Fig. 11 [7]:

$$F = \frac{n^2\pi^2 EI}{L^2}. \qquad (3-34)$$

$$v = \mathrm{B}\sin\frac{n\pi x}{L}. \qquad (3-35)$$

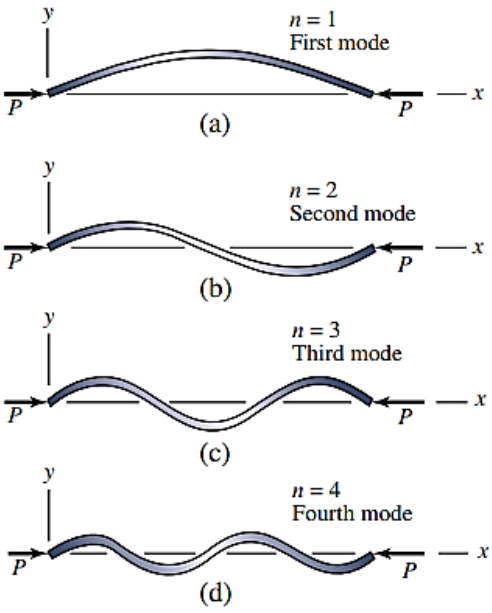

Fig. 11 Deflection distributions for increasing values of n [7]

3.4.3. Euler's Buckling Load for other boundary conditions

Some of the other end conditions that can be applied to a slender column is shown in Fig. 12 and their Euler's buckling load is given by

$$F = \frac{n^2\pi^2 EI}{KL^2}. \qquad (3-36)$$

Where K is the column effective length factor and its values are given in Fig. 12.

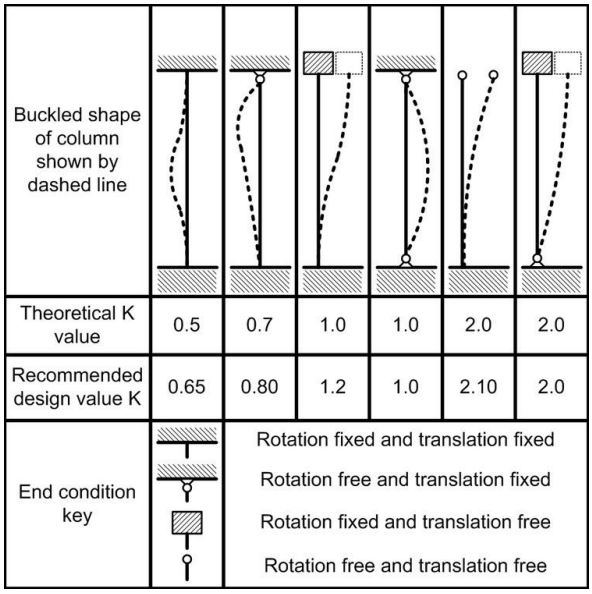

Fig. 12 Mode of failure of a slender column with different boundary conditions

3.4.4. Eigenvalue Buckling with ANSYS®

The search for the load that can cause structural instability and bifurcation is known as buckling load. The finite element equilibrium equations for this type of analysis involve the solution of homogeneous algebraic equations whose lowest eigenvalue corresponds to the buckling load, and the eigenvector represents the primary buckling mode. Eigen value buckling is used to calculate the theoretical buckling load of a linear elastic structure. Since, it assumes the structure exhibits linearly elastic behavior, the predicted buckling loads are overestimated (unconservative). This is available for valid structural degrees of freedom only and the structure fails suddenly with a horizontal force deflection curve. The structure is considered to have constant stiffness effects [6].

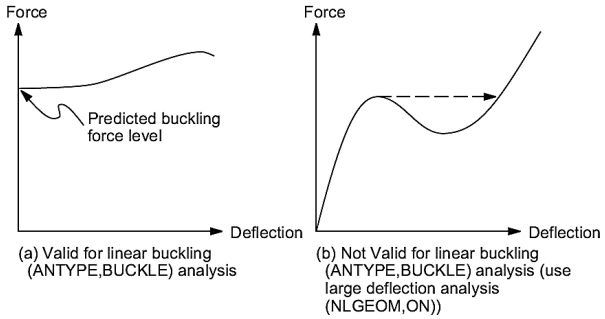

Fig. 13 Types of buckling problems [6]

A static solution is needed to establish the stiffening of the structure under the applied load (stress stiffening). There are several buckling modes (theoretically, infinitely many!) in a structure. The first buckling mode is the one requiring the smallest load. A linear structure with a force buckling curve like Fig 13a is well modelled by a linear buckling analysis, whereas for curve like Fig 13b, a large deflection analysis is appropriate (with large deflection ON). The buckling problem is formulated as eigenvalue problem [6]:

$$([K] + \lambda_i[S])\{\psi_i\} = 0, \qquad (3-37)$$

where:

$[K]$ = Stiffness matrix

$[S]$ = Stress matrix

λ_i = ith eigenvalue (used to multiply loads generated in $[S]$

ψ_i = ith eigenvector of displacements

The eigenvectors are normalized so that the largest component is 1.0. Thus, the stresses (when output) may only be interpreted as a relative distribution of stresses. By default, the Block Lanczos and Subspace Iteration methods find buckling modes in the range of negative infinity to positive infinity [6].

3.5. Non-linear Structural Analysis

This is a good tool to confirm the buckling load of a structure, when there is a small deformation in the structure due to some unknown external factors or when the structure is already deformed due to known or unknown factors. In this case, large deflection methodology or arclength method can be applied to model the sudden large displacement in a structure due to buckling.

4. 1.3 GHz SRF Cavity Assembly FEA

The stress and buckling analysis is performed on a 3-cell 1.3-GHz Niobium SRF cavity with its Titanium jacket, its structure is as shown in Fig. 14. The cavity shape and Titanium jacket is similar to Tesla-like that was designed at KEK. This simulation is just an example and should not be considered as the finalized results for the stress and buckling analysis for Tesla-like cavity.

4.1. Static Structure Analysis

For the high-pressure gas safety authority the SRF cavity with its Titanium vessel should be able to withstand maximum allowable working pressure (MAWP) of 0.2 MPa or 2 bar absolute pressure. The cavity normal operating pressure is 0.003 MPa or 0.03 bar absolute, which is roughly the saturated vapor pressure of 2.0 K superfluid helium. Moreover, since this design and the materials used for this assembly are not standardized the design must be proven robust. For this design, the simulation is divided in three case studies:

- *Case A*: In this case the assembly is in room temperature condition (40 °C) with helium gas between the SRF cavity and Ti jacket. The MAWP between the SRF cavity and Titanium Jacket is 0.2 MPa and the tuner displacement is 0.65 mm. The location of tuner displacement

can be seen in Fig. 14. The displacement is considered equally on either jackets, hence, 0.325 mm on one jacket and -0.325 mm on the other tank. There is vacuum outside Ti jacket and inside SRF cavity.

- *Case B*: In this case, the assembly is cooled down to operational conditions by filling superfluid helium between the SRF cavity and its Ti helium jacket, i.e, it is cooled down from 40 °C to -271.4 °C (1.8 K). The MAWP between the SRF cavity and Ti Jacket is 0.2 MPa and the tuner displacement is 0.65 mm. There is vacuum outside Ti jacket and inside of the SRF cavity.

- *Case C*: In this case, the assembly is cooled down to operational conditions by filling superfluid helium between the SRF cavity and its Ti helium jacket, i.e, it is cooled down from 40 °C to -271.4 °C (1.8 K). The MAWP between the SRF cavity and Titanium helium Jacket is 0.2 MPa and the tuner displacement is maximized to 3 mm. There is vacuum outside Ti jacket and inside the SRF cavity.

The layout of the cases in ANSYS® Workbench is shown in Fig. 15 and each component is described in detail in next sections.

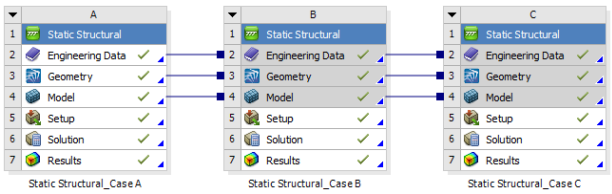

Fig. 15 3-cell 1.3 GHz Tesla-like cavity with its Titanium jacket

4.1.1. Engineering Data

In this section, the necessary material properties are inserted to provide necessary information regarding the elastic and plastic behavior of the materials. Examples of some of the included properties are Young's modulus, Poisson's ratio, Shear modulus, Coefficient of thermal expansion etc. It is possible to vary properties with respect to temperatures too either in tabular or in equation form.

For this simulation, we will only consider the elastic properties of Nb and Ti. The properties that were entered in the engineering data are shown in Fig. 16 and the properties are also listed in table 1:

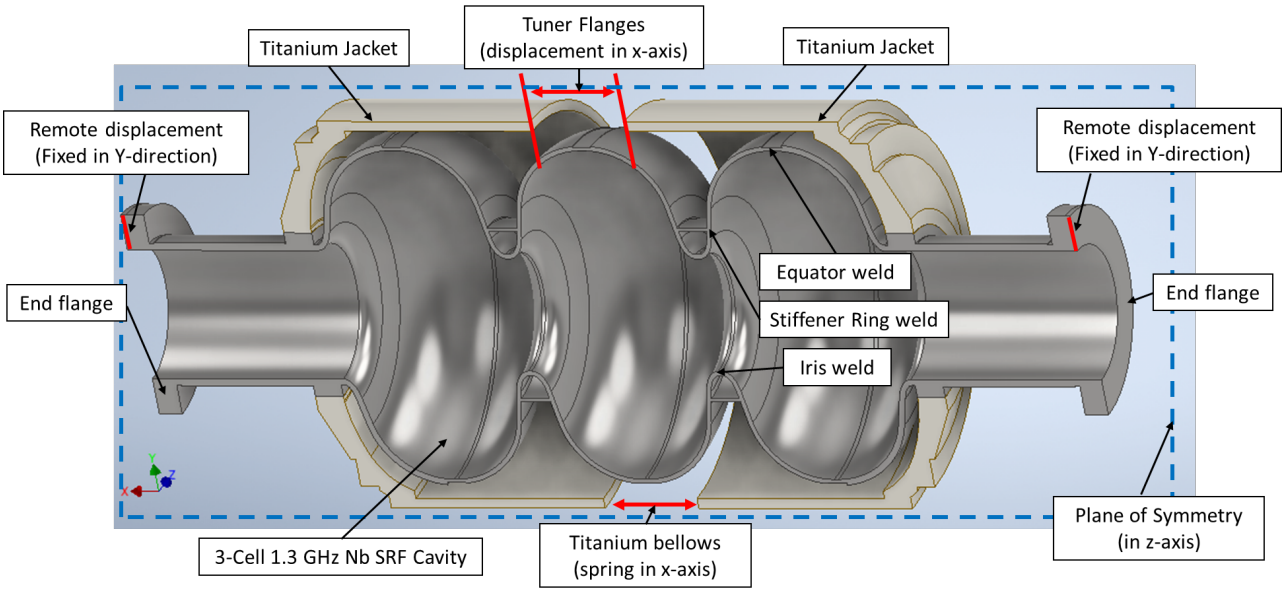

Fig. 14 3-cell 1.3 GHz Tesla-like cavity with its Titanium jacket

Table 1 Mechanical properties of Nb and Ti

Properties	Unit	Nb	Ti
Young's Modulus	GPa	103	107
Poisson's Ratio	-	0.38	0.32
Coeff. of Thermal Expansion	$\times 10^{-6}$ /°C	4.87	5.22

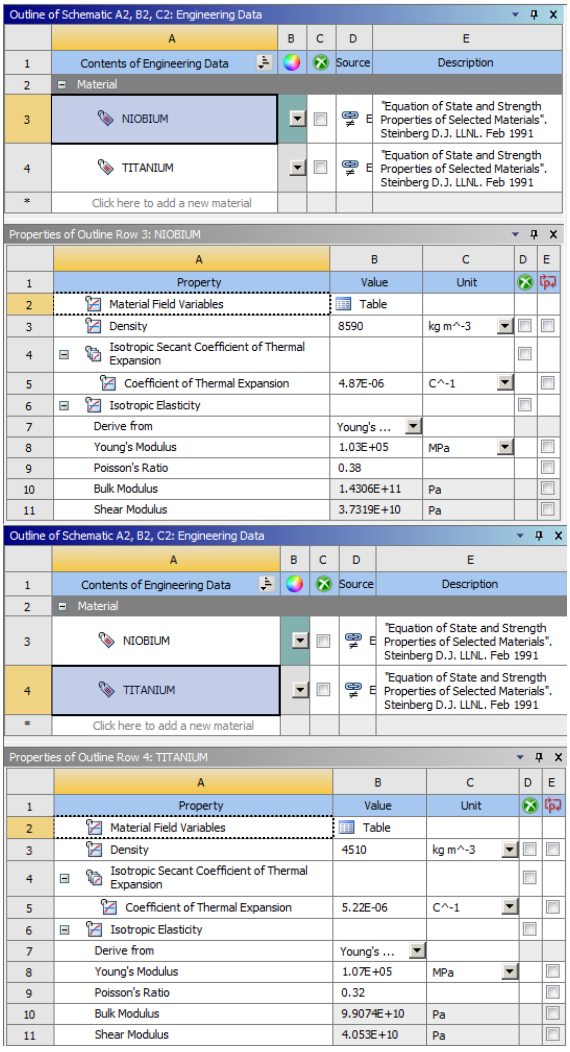

Fig. 16 Engineering data for Nb and Ti

4.1.2. Geometry

In this section, the accurate CAD model of the geometry that needs to be analyzed is uploaded. To draw the CAD model there is an internal CAD modeler 'Spaceclaim®' that can be utilized or there are many CAD modelling software's such as Solidworks®, AutoCAD®, Autodesk Inventor®, Catia® etc. The CAD model can be uploaded to the geometry directly by converting it in compatible formats. In this section, usually the important sub-sections that needs to be taken care of is the global controls, as if the meshing has to be shared throughout the multipart body or not. If it is set to 'share' then the connection between multipart bodies will be considered contact regions without any respective movement to each other (as if it was perfectly welded).

The half 3-D model for 1.3 GHz 3-cell SRF cavity was drawn in Autodesk Inventor and uploaded in the Geometry section, as shown in Fig. 17.

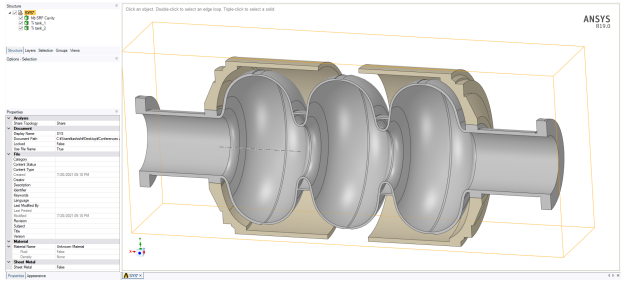

Fig. 17 Half-3D CAD model of 3-cell 1.3 GHz SRF cavity in ANSYS® Geometry

4.1.3. Model

In this section, the necessary material assignments, types of connections, symmetry (if exists) and meshing is conducted. The uploaded CAD geometry is discretized using various methodologies available in the ANSYS® Meshing software. This is the most important and sensitive stage of the simulation, as the simulation results can vary widely due to mesh size. Hence, for every CAD geometry mesh dependency study needs to be conducted to determine the minimum mesh size below which the percentage change is less than 1% between

subsequent simulations in the quantities such as stress, strain, deformation etc.

- *Geometry*: All the solids or surface geometries are listed here. The materials are assigned to individual solids, as shown in Fig. 18. The cavities are assigned Niobium and the jackets are assigned Titanium.

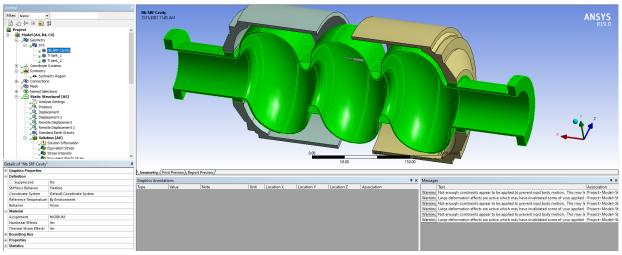

Fig. 18 Material assignment in ANSYS® Model

- *Symmetry*: This is an optional setting. As the cavity and tank structure can be considered axi-symmetrical, only a half 3D model of the structure was modeled, and the other half was considered as a symmetry. In this case, the model is symmetrical in z-axis and the faces in red are with which the cavity model is symmetrical to, as seen in Fig. 19.

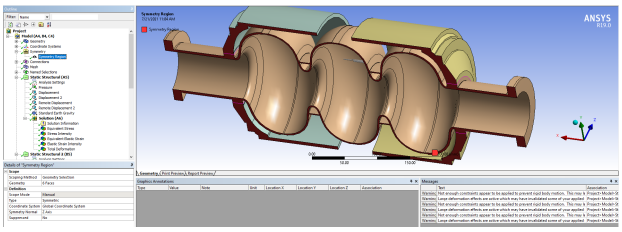

Fig. 19 Symmetry region for the half 3D model (in red)

- *Meshing*: In this section, the uploaded CAD geometry is discretized using hexahedral meshes. Mesh dependency studies have to be carried out and the maximum possible size of the meshes were determined. In this case the maximum mesh size was selected to be 3 mm. The geometry was discretized in to 87,440 number of elements and 470,000 nodes, as shown in Fig. 20.

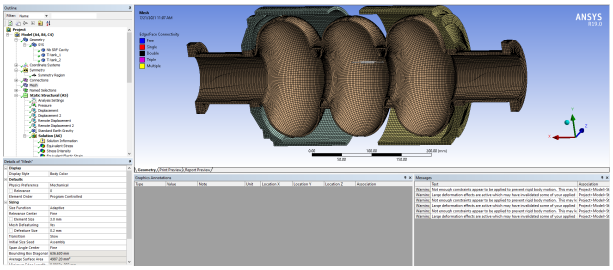

Fig. 20 Discretization of the geometry by meshing

4.1.4. Setup

In this section, the external factors and boundary conditions are provided to the model. The analysis settings and boundary conditions are shown in Fig. 21:

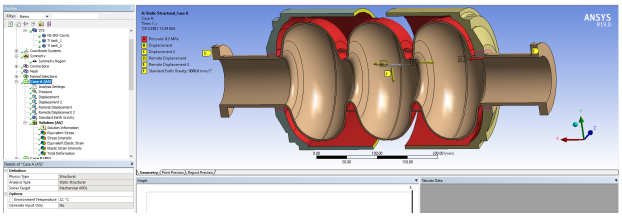

Fig. 21 Boundary conditions and analysis settings

- *Analysis settings*: In this section, we can basically set the number of steps, switching large deflection ON or OFF for non-linear structural analysis and other controls, as shown in Fig. 22.

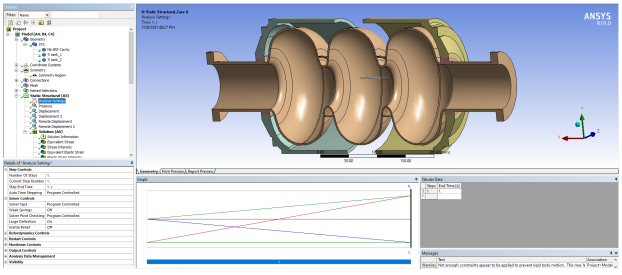

Fig. 22 Analysis settings for the simulation

- *Pressure*: The inner faces of the Ti jacket and the outer faces of the SRF cavities are selected to provide pressure condition normal to them.

For all cases, pressure was set to 0.2 MPa, as seen in Fig. 23.

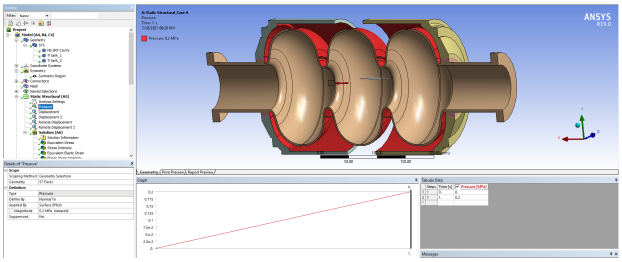

Fig. 23 Pressure boundary condition (in red)

- *Displacement*: This is provided to the cross-sectional inner surface of the Tank 1 and Tank 2, respectively, as seen in Fig 24, to simulate the tuner movement, which stretches the cavity structure. There is a virtual spring with a stiffness coefficient of 206 N/mm connecting these surfaces, which replaces the Ti bellow (added in connection setting). Displacement condition can used to fix or provide movement to a line or surface in any direction. In this case, the cavity was stretched in ±x-axis and the cavity movement in other directions were kept free to deform or move.

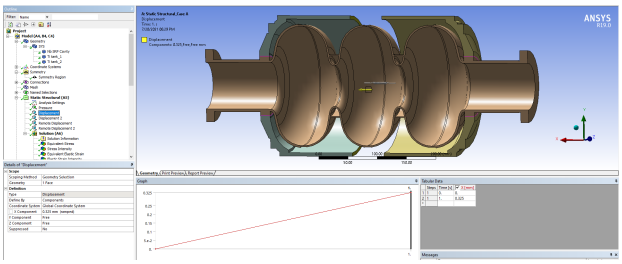

Fig. 24 Displacement boundary condition

- *Remote Displacement*: This was not used to provide any displacement but to fix the end flanges in Y-direction. As the cavity structure is in a string in a cryomodule and is connected to another cavity structure with a bellow assembly, as seen in Fig. 1, it cannot be fixed in all three directions of the space. Hence, only a line contact is fixed in Y-direction and no rotation is allowed along any direction, as shown in Fig. 25.

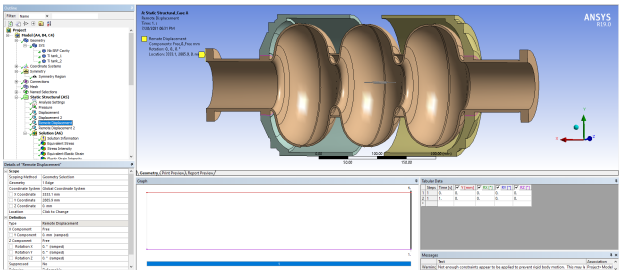

Fig. 25 Remote displacement boundary condition

4.1.5. Solution and Results

In this section, the results of the converged solution are shown. It is possible to view and plot many of the quantities such as Von-misses stress, Von-misses strain, Stress intensity, Deformation (total or directional), strain energy, linear stress etc. Moreover, with a probing tool it is possible to determine all of the above listed quantities at a node, element, line or a plane. Usually, the results are visually represented in a gradient color format but that can be modified according to designers' preference. It is possible to form charts, graphs and many other graphical and visual form of the simulation results.

The stress intensity on the cavity assembly for Cases A, B and C are shown in Fig. 26 and summarized in Table 2 and 3. The maximum stress intensity in all cases occurred at the stiffener ring weld section. It is mainly due to the stretching effect on the cavity from tuner displacement. For the high-pressure gas safety regulations, the mechanical properties of the materials used to manufacture the pressure vessel should satisfy the following conditions: > 1.5 times the maximum stress intensity for 0.2% Y.S and > 4 times the maximum stress intensity for T.S, on individual components.

Table 2 Maximum stress intensity on various components of cavity assembly

Case	Nb Half Cells [MPa]	Ti Tank [MPa]	Nb-Ti weld [MPa]
A	70	5	12
B	76	5	23
C	300	18	65

Table 3 Maximum stress intensity on various sections of SRF cavity

Case	Stiffener Ring Weld [MPa]	Iris Weld [MPa]	Equator Region weld [MPa]
A	147	22	12
B	161	24	14
C	668	111	67

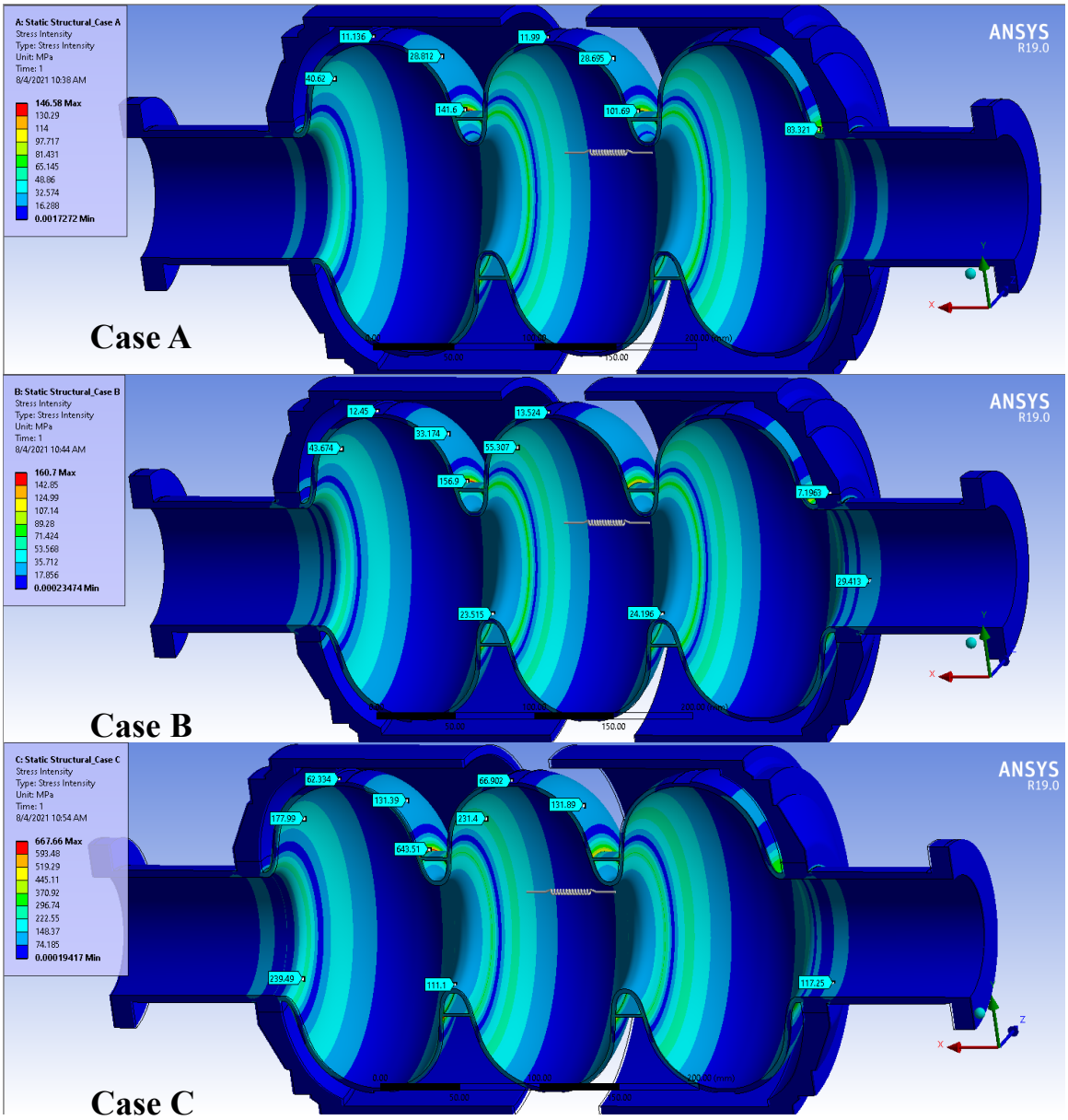

Fig. 26 Stress intensity on the cavity assembly for various cases

4.2. ANSYS® Eigenvalue Buckling

In this FEA, we would determine the pressure at which the cavity structure will buckle. As theorized before this analysis only takes the elastic region of the materials in consideration. For this analysis, Case B is taken into consideration, as the tuner movement is the least out of all cases and the cavity structure would be easier to buckle in Case B rather than Case C, as larger tuner movement makes the cavity structure more difficult to buckle. The case structure of Eigenvalue buckling in ANSYS® is shown in Fig. 27.

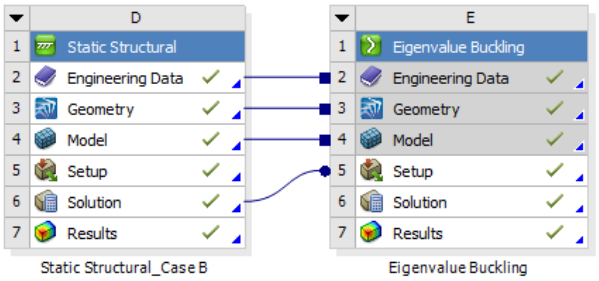

Fig. 27 Case structure of Eigenvalue buckling simulation

4.2.1. Engineering Data

In this case, the engineering data is the same as in static structure analysis, as the engineering data is linked, the elastic mechanical properties are transferred to the geometry for Eigenvalue buckling system.

4.2.2. Geometry

The geometry remains the same as the geometry considered for the static structure analysis. Hence, the same geometry is forwarded to this system by linking them.

4.2.3. Model

As the same geometry is transferred from the static structure analysis system, the model with its meshing and connections are also transferred to eigenvalue buckling system.

4.2.4. Setup

In this case, the same boundary conditions were transferred to the eigenvalue buckling system. However, the pressure boundary condition is suppressed as it would be considered as a variable on each nodes of outer surface of SRF cavity and inner surface of Ti helium jacket, to determine the buckling pressure of the SRF cavity structure. The various boundary conditions are shown in Fig 28.

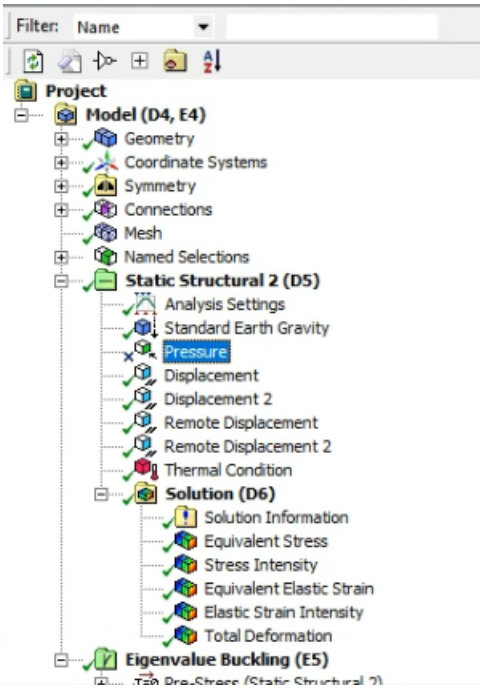

Fig. 28 Boundary condition for structure analysis for buckling simulation

4.2.5. Analysis Settings for the Solver

Mechanical APDL solves the governing equations for Eigenvalue buckling analysis. The pre-stress load pattern is set to No, since we would like to provide pressure as the variable to determine the load multiplier to the initial pressure condition of 0.2 MPa. In this case, we would like to determine 2 modes of failure,

hence maximum number of modes to find are set to 2, as seen in Fig. 29.

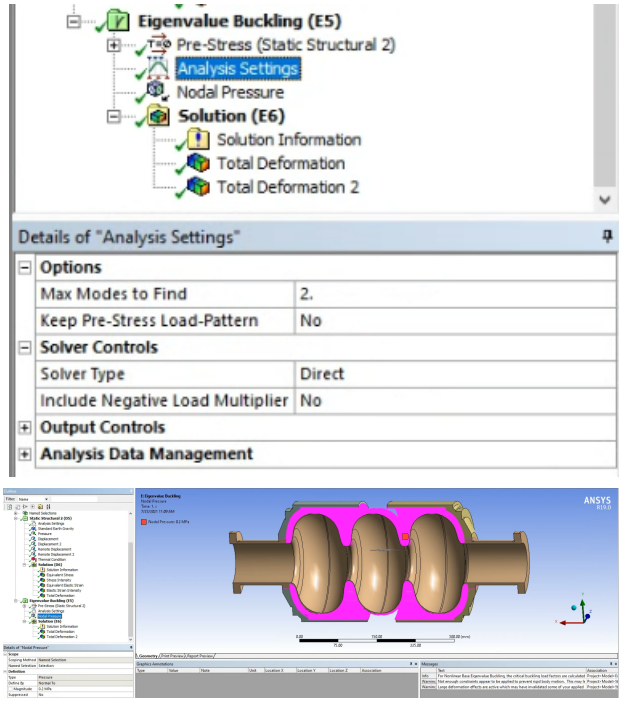

Fig. 29 Analysis setting (top) and nodal pressure boundary condition (below)

4.2.6. Results and discussions

The buckling load multiplier for the cavity structure was determined to be 385.2 for the 1st Eigen mode and 386.6 for the 2nd Eigen mode, as seen in Fig. 30. This provides the buckling pressure of 77.1 MPa (385.2 × 0.2 MPa) for both Eigen modes. As the mode of failure were at the sections of similar thickness and similar in nature, the load multipliers were equal to each other. The buckled behavior of the structures can be seen in Fig. 31.

For a 9-cell cavity, the 1st mode of Eigenvalue buckling occurs at 48 MPa with similar boundary conditions. The mode of failure for a 9-cell cavity structure is similar to the one shown for 3-cell cavity structure.

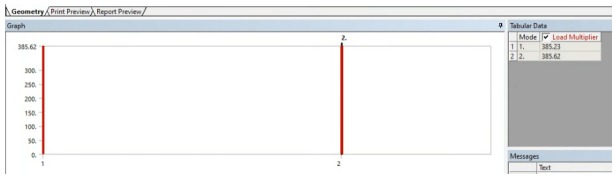

Fig. 30 Load multiplier for the buckling modes

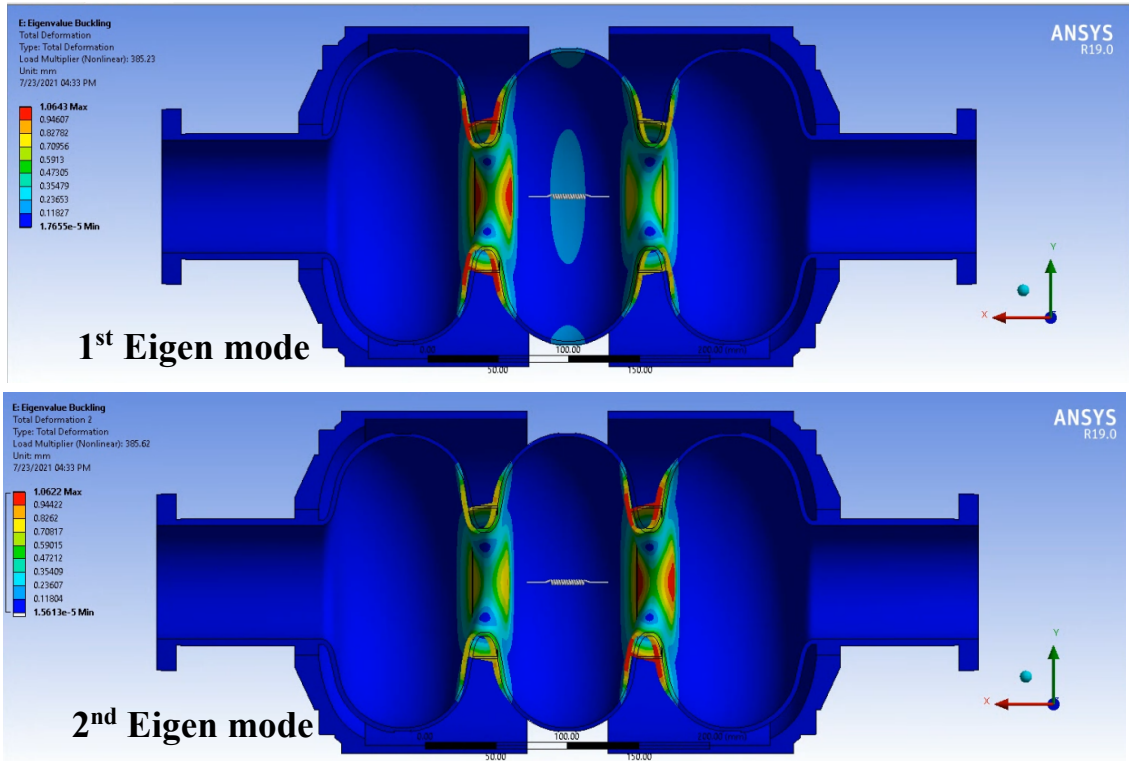

Fig. 31 Load multiplier for the buckling modes

4.3. Non-linear Structural Analysis

This analysis is conducted to verify the results obtained from the Eigen value buckling analysis, and to study the effect of deformations in the cavity structure on its buckling pressure. In this study, the buckled structure from Case B was considered for a non-linear structural analysis with large deflection set to ON to determine the buckling pressure.

4.3.1. Case structure

The case structure for this simulation is a continuation of the Eigen value buckling analysis, where any of the determined buckling mode can be transferred to a static structure analysis. Moreover, it is possible to control the level of buckling in the structure that would be transferred with scale factor, which can be varied from 0 to > 1, where 0 being the original structure and 1 being the buckled structure that would be transferred to the static structure analysis. Here, the 1st Eigen mode was transferred to four static structure analysis studies with the scale factors being varied from 0.005, 0.01, 0.1 and 1, as shown in Fig. 32.

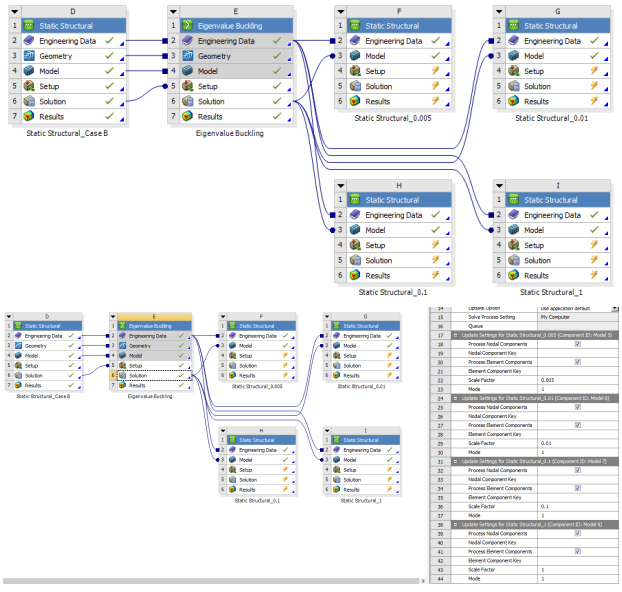

Fig. 32 Case structure for non-linear structural analysis

4.3.2. Boundary Conditions

The boundary conditions remained the same as the ones previously used for structure analysis of Case B, except the pressure boundary condition, which was incrementally increased from 0 – 80 MPa in 8 steps to determine the buckling pressure, as shown in Fig. 33. At the buckling pressure, the solution will not converge due to large deformation of the structure, as seen on Fig. 34.

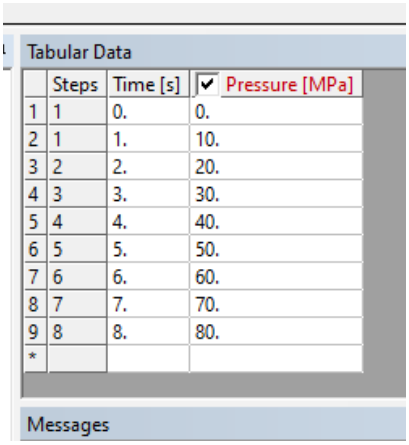

Fig. 33 Incremental pressure boundary condition

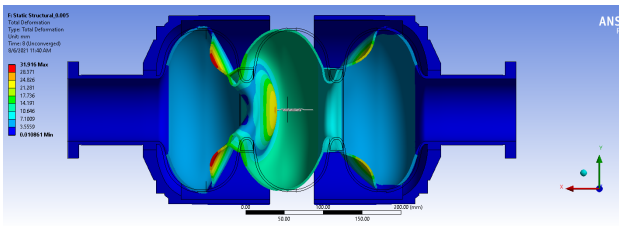

Fig. 34 Buckled cavity structure

4.3.3. Results and Discussions

The buckling pressure was determined by placing a total deformation probe on a point on the cavity structure where the maximum buckling occurs. The location of the deformation probe is shown in Fig. 35. The total deformation obtained from the deformation probe was plotted against the pressure condition for

various scaling factors and is shown in Fig. 36. The buckling pressure was 74 MPa for a structure with scale factor of 0.005 and approximately 54 MPa for the scale factor of 1. From the plot it can theorized, that for elastic material properties, the cavity will not buckle upto 54 MPa pressure. The buckling pressure usually should be > 4 times the MAWP, and in this case the cavity structure has sufficient strength to qualify for that criterion.

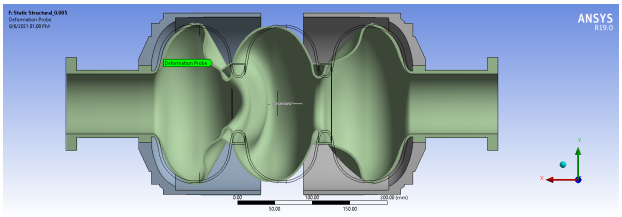

Fig. 35 Deformation probe location on the structure after buckling for scale factor of 0.005 at 73.5 MPa pressure

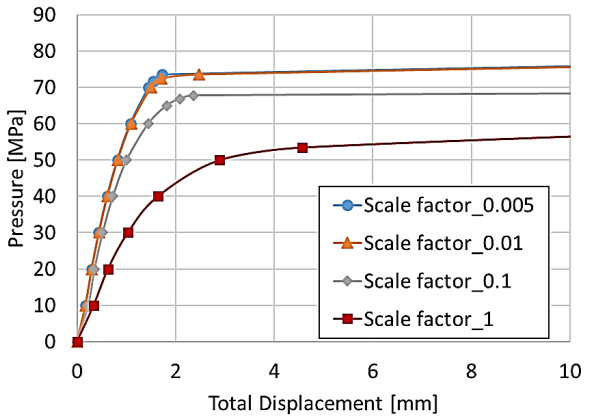

Fig. 36 Pressure v/s total displacement for the deformation probe on the Nb SRF cavity

5. Summary

In this lecture, the basics of finite element analysis for static structure and buckling failure was detailed. An example of 3-cell 1.3 GHz Tesla-like cavity was considered to determine the stress generated on the cavity for the high-pressure gas safety conditions (the results are different for 9-cell cavity). Moreover, the buckling pressure and its Eigen modes were determined.

REFERENCES

[1] A. Yamamoto et al., "Ingot Nb based SRF technology for the International Linear Collider", *AIP Conference Proceedings* 1687, 030005 (2015); doi:10.1063/1.4935326

[2] The International Linear Collider: A Global Project, arXiv:1903.01629 [hep-ex]

[3] AIP Conference Proceedings 1434, 1575 (2012); https://doi.org/10.1063/1.4707088

[4] B. Aune et al., "Superconducting TESLA Cavities", *Phys. Rev.ST Accel. Beams* 3, 092001 (2000)

[5] E Madenci and I Guven., The finite element method and applications in engineering using ANSYS®, second edition, Springer 2015.

[6] P. Kohnke, ANSYS® Mechanical APDL theory reference, ANSYS® Inc.

[7] A. Bedford and K.M Leichti, Mechanics of materials, second edition, Springer.